

# Frequency conversion in a hydrogen-filled hollow-core fiber using continuous-wave fields

Anica Hamer and Simon Stellmer\*

*Physikalisches Institut, Rheinische Friedrich-Wilhelms-Universität Bonn, Bonn, Germany*

Frank Vewinger

*Institut für Angewandte Physik, Rheinische Friedrich-Wilhelms-Universität Bonn, Bonn, Germany*

Thorsten Peters

*Technische Universität Darmstadt, Darmstadt, Germany*

Michael H. Frosz

*Max-Planck-Institut für die Physik des Lichts, Erlangen, Germany*

(Dated: September 4, 2024)

In large-area quantum networks based on optical fibers, photons are the fundamental carriers of information as so-called flying qubits. They may also serve as the interconnect between different components of a hybrid architecture, which might comprise atomic and solid state platforms operating at visible or near-infrared wavelengths, as well as optical links in the telecom band. Quantum frequency conversion is the pathway to change the color of a single photon while preserving its quantum state. Currently, nonlinear crystals are utilized for this process. However, their performance is limited by their acceptance bandwidth, tunability, polarization sensitivity, as well as undesired background emission. A promising alternative is based on stimulated Raman scattering in gases.

Here, we demonstrate polarization-preserving frequency conversion in a hydrogen-filled anti-resonant hollow-core fiber. This approach holds promises for seamless integration into optical fiber networks and interfaces to single emitters. Disparate from related experiments that employ a pulsed pump field, we here take advantage of two coherent continuous-wave pump fields.

## I. INTRODUCTION

Highly efficient and state-preserving single-photon frequency conversion is a prerequisite for the realization and operation of quantum computing and communication in a hybrid architecture with optical interconnections [1–12]. The two most well-known methods for quantum frequency conversion rely on the  $\chi^{(2)}$  nonlinearity of crystals [2, 3, 5–9] and the  $\chi^{(3)}$  nonlinearity of atomic gases in combination with short-pulse lasers [13–16]. Developments based on the  $\chi^{(2)}$  nonlinearity of crystals have reached near-unit conversion efficiency and a drastically reduced incoherent background. Still, the  $\chi^{(3)}$  nonlinearity of molecular gases offers many benefits, as it sidesteps some of the limitations inherent to crystals, among them a very narrow acceptance bandwidth, polarization-dependence of the conversion process, absorption, heat management, and background emission.

In recent work, coherent Stokes and anti-Stokes Raman scattering (CSRS/CARS) processes based on the  $\chi^{(3)}$  nonlinearity in gases have been demonstrated for frequency conversion [17–20]. These processes are intrinsically broadband, insensitive to the input polarization, and can operate on a wide selection of molecules and their transitions [10, 21, 22].

In this Letter, we present frequency conversion from 863 nm to 1346 nm based on CSRS process inside an antiresonant-reflecting hollow-core fiber (ARR-HCF). While the process itself has already been established [21, 23], we here show that the mode confinement increases the conversion efficiency. Remarkably, the fiber does not deteriorate preservation of polarization, and interaction with the glass structure does not induce undesired Raman scattering. To our knowledge, all related experiments to date employed pulsed lasers to generate the coherence. By contrast, here we employ a pair of precisely adjusted continuous-wave (cw) lasers to drive the conversion process. This approach broadens the scope of applications to cases where the arrival time of the probe photon is unknown. Importantly, applications involving atoms or ions require photons with a narrow linewidth to match an electronic resonance and are incompatible with short-pulse lasers [24].

The ARR-HCFs are a sub-group of the hollow-core photonic crystal fiber (HC-PCF), which are based on the guiding of the leaky mode through the eponymous hollow core [25]. Common implementations are named revolver-type fibers or single-ring PCFs and feature a small number of capillaries arranged around the hollow core at consistent azimuthal distances within a jacket capillary [26, 27]. The advantages of these fibers include an optical nonlinearity for the propagating mode combined with a tunable dispersion using a gas filling [28]. Their properties are determined by the dimensions and arrangement of the holes. A combi-

---

\* Correspondence email address: stellmer@uni-bonn.de

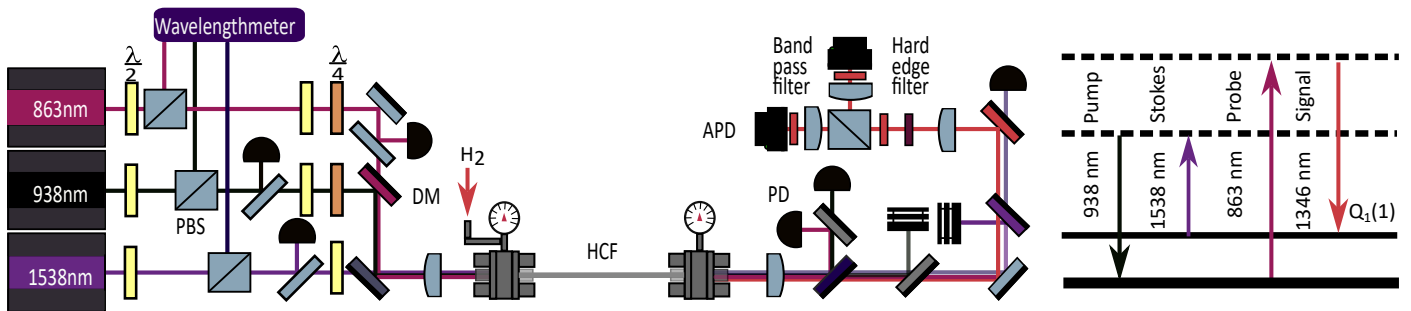


Figure 1. Experimental setup. Two fields at 938 nm (pump) and 1538 nm (Stokes) are overlapped with the probe light at 863 nm via dichroic mirrors (DM) and focused into the hydrogen-filled hollow core fiber (HCF). Behind the fiber, the converted light (signal, 1346 nm) is separated from the input light. Two avalanche photon detectors (APDs) record the s- and p-polarized components after a polarizing beam splitter (PBS). The schematic diagram shows the underlying CSRS process.

nation of their outstanding polarization-maintaining property [29], high damage threshold, large interaction length, low transmission loss, and tunable dispersion essential for phase matching in CSRS processes [30] make these fibers ideal candidates for four-wave mixing processes [10, 31–35]. See Ref. [36] for a recent review.

## II. EXPERIMENTAL SETUP

We perform frequency conversion from 863 nm to 1346 nm, where the choice of wavelengths is motivated by the potential conversion of the two entangled photons of the biexciton emission of indium arsenide (InAs)/gallium arsenide (GaAs) quantum dots [37–40] to the telecom O-band. The frequencies of two fields near 938 nm and 1538 nm are adjusted such that their beat note matches the vibrational transition at 125 THz within the  $Q_1(1)$  branch of molecular hydrogen. The resulting nonlinear polarization is probed with the light field at 863 nm, leading to the emission at 1346 nm.

A schematic diagram of the experiment and the underlying conversion is shown in Fig. 1. The pump laser light at 938 nm is provided by an amplified diode laser, while the 1538 nm Stokes light originates from a diode laser combined with a fiber amplifier. These two lasers are stabilized at the MHz level using a wavelength meter, their power levels are adjusted to 50 mW. In the following, pump and Stokes field are called pump fields. The probe photons are simulated using a diode laser operating at 863 nm at a power level much smaller than the pump fields. The power levels of the three lasers are monitored, and their polarizations can be adjusted individually.

All beams are overlapped using dichroic mirrors and focused into the fiber with an achromatic lens. Each end of the fiber is glued into a centering piece, which in turn is mounted into a home-built, stainless steel, hermetically sealed, cylindrical high-pressure chambers using an O-ring seal. The vessels are tested up to 700 bar. AR-coated sap-

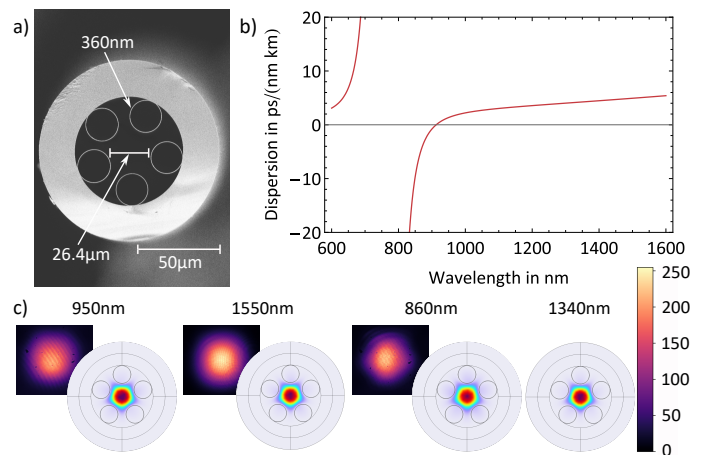


Figure 2. a) SEM image of the fiber facet. b) Dispersion of the fiber, calculations based on Ref. [41]. c) Mode propagation inside the fiber with a finite element simulation, showing the norm of the amplitude of the electric field inside the fiber and images of the mode behind the fiber for different wavelengths.

phire windows are sealed to the vessels using O-rings. Behind the fiber, the converted photons at 1346 nm are separated from the input light fields using dichroic mirrors and are guided to a polarizing beamsplitter (PBS) and two avalanche photodiodes (APD, ID Qube NIR, dead time 1  $\mu$ s) with a quantum efficiency of 12.5%. Spectral filtering is achieved through bandpass filters (10 nm width and 93% transmission) and an edge filter at 1300 nm with 97.7% transmission.

We employ a single-ring ARR-HCF. The core has a diameter of 26.4  $\mu$ m and is surrounded by five capillaries with a wall thickness of 360 nm, as shown in Fig. 2 a). The fiber is 27 cm long. To calculate fiber properties such as the mode field diameter or the transmission bandwidth depending on the chromatic dispersion, we use the model given by Zeisberger-Hartung-Schmidt [41] to obtain the effective refractive index  $n_{\text{eff}}$  inside the fiber core.

The calculation of  $n_{\text{eff}}$  allows us to determine if the fiber can support the relevant wavelengths. Coupling between the core modes and the capillary resonances [10, 41] leads to resonances in the group velocity dispersion, as shown in Fig. 2 b). These resonances are associated to loss, and the wall thickness  $w$  of the capillaries must be chosen such as to shift the singularities away from the wavelengths used in the experiment.

We also perform simulations of mode propagation inside the fiber using the finite element simulation software *Comsol*. All wavelengths relevant to this work are supported by the fiber. Simulated mode profiles and images of the Gaussian  $\text{HE}_{11}$  fiber modes are shown in Fig. 2 c).

Losses in hollow-core fibers can be attributed to various sources: leakage losses, imperfection losses, and material absorption of the fiber [28], as well as absorption by the hydrogen molecules [31]. Possible bend losses can also occur, but are negligible here. Leakage losses and material absorption [28, 30] are suppressed by the choice of the fiber with its resonance wavelengths, and imperfection losses only play a significant role for visible and ultraviolet wavelengths [28]. For the type of fiber used here, coupling efficiencies in excess of 90% have been obtained [42], but this value has been reduced to 30% in the high-pressure vessel after filling with hydrogen.

### III. FREQUENCY CONVERSION

#### A. Role of the gas pressure

The nonlinear conversion needs to fulfill the phase matching condition  $\Delta\beta = -\beta_{938\text{nm}} + \beta_{1538\text{nm}} + \beta_{863\text{nm}} - \beta_{1346\text{nm}}$ . We perform a calculation of the conversion efficiency in dependence of gas pressure. Starting from the propagation constant  $\beta = 2\pi\nu/c \cdot n_{\text{eff}}(p, \lambda)$  and taking  $n_{\text{eff}}$  depending on the pressure  $p$  and the wavelength  $\lambda$  from the Zeisberger model [41], we find an oscillatory behavior with a peak efficiency near 250 bar, shown as the solid curves in Fig. 3.

In the experiment, we analyze the molecular resonance of the CSRS process by scanning the relative detuning of the two pump fields. We find that the pressure-dependent lineshapes, linewidths, and collisional shifts [43–45] are identical to our previous work on a bulk hydrogen gas [21, 23].

The conversion efficiency is pressure-dependent and scales as [17]:

$$I_{1346} \propto |\chi^{(3)}(\omega)|^2 L^2 \text{sinc}^2\left(\frac{\Delta\beta(p) \cdot L}{2}\right) I_{938} I_{1538} I_{863}, \quad (1)$$

where  $\chi^{(3)}(\omega)$  denotes the third-order nonlinear susceptibility,  $L$  the interaction length, and  $\Delta\beta$  is the previously mentioned pressure-dependent phase matching condition included in a squared sinc function. The raw count rates, which are proportional to the efficiency, are shown in Fig. 3.

In the regime of low pressures of up to about 20 bar, the data nicely follows the model; Fig. 3 (right column). For the first maximum at 12(1) bar and the previously described experimental parameters, we obtain an internal conversion efficiency of  $2.4 \times 10^{-11}$  (relative efficiency  $9.6 \times 10^{-7} \%/W^2$ ). After scaling by the power of the pump fields used, this is an improvement by two orders of magnitude compared to our previous work in a bulk gas [23]. In the current experiment, we refrained from a drastic increase in pump powers to not damage the fiber.

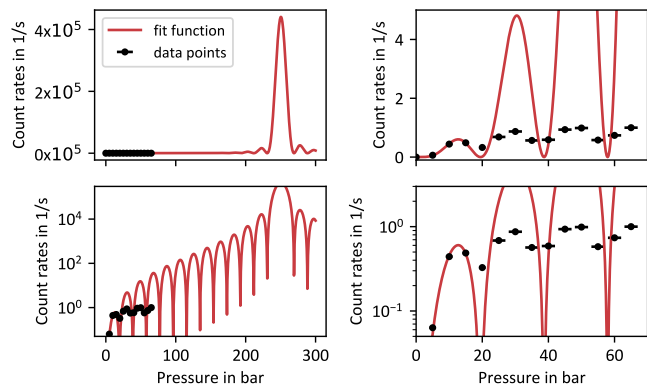


Figure 3. Pressure-dependent count rates, shown here for different pressure ranges (left and right column) and presented on a linear (top) and semi-logarithmic (bottom) scale. The data (black points) follows the calculation (solid red curve) only for low pressure; see the text for details.

The count rate follows an oscillatory behavior with the same periodicity as predicted by the model. For higher pressures above about 20 bar, however, the measured efficiency falls significantly short of expectations and does not closely follow the model. While the model does neglect subtle effects such as backcoherence [10], higher order Stokes shifts [33], and intermodal conversion [33], we here discuss two explanations for the saturation in conversion efficiency at large gas pressure.

Firstly, we experimentally observe significant gas losses occurring at pressures above 20 bar, leading to a pressure gradient along the fiber. We therefore only use data up to 20 bar for the fitting routine. The inhomogeneous pressure, possibly along with the gas flow through the fiber, disrupts coherence along the length of the fiber and thus limits the efficiency. This observation is verified in simulations. In future work, a uniform pressure within the fiber will be recovered by placing the entire fiber inside a high-pressure vessel.

Secondly, and conceptually more relevant, the intensity provided by the two cw pump fields might be insufficient to generate a sufficiently strong coherent wave of optical phonons which behave as stationary oscillators [46] and drive the conversion process. Previous experiments [10,

36] employed pulsed lasers with substantially higher peak intensities. Additionally, in the approach described here, the Stokes photon was not generated by stimulated Raman scattering (SRS), but was instead provided by a laser as well. A redesign of the optics will allow us to improve on the fiber coupling efficiency, which in turn will allow us to increase the pump fields and elucidate the build-up of coherence with increasing pump power.

### B. Preservation of polarization

Quantum frequency conversion requires preservation of the incoming photon state, particularly the polarization. Since the hydrogen gas itself is isotropic, the reference frame of the system is determined by the light field. We tested the preservation of polarization by measuring the projection of the output state for both linear and circular polarizations. To this end, the polarization of the probe light is varied, and a polarizing beamsplitter (PBS) separates the V and H polarizations of the converted light onto two separate detectors. Silver mirrors are used to maintain the polarization, and the optics were characterized by means of a test beam near 1310 nm.

For all values of linear and circular polarization, the converted light faithfully follows the input polarization. To calculate the fidelity, the background-corrected data is fitted to sine functions. We obtain a value of 96% for linear polarization and 84.5% for circular polarizations, leading to an overall fidelity of above 0.91. This value can be fully explained by imperfect polarization optics and allows us to conclude that the fiber does not deteriorate the polarization measurably [29].

### C. Background noise

Frequency conversion in crystals is often plagued by undesired Raman scattering into the spectral band of the converted photons. These processes are driven through the crystal material, and there is justified hope that such processes are suppressed or removed entirely in the case of a gas-filled hollow-core fiber where the glass structure has minimal overlap with the light fields. Indeed, we do not observe any background near the target wavelength of 1346 nm that would originate from either of the two pump fields or their combination.

When increasing the power of the 863-nm probe field to the level of a few 10 mW, however, we do observe weak emission near 1346 nm that scales linearly with both the power of the 863-nm field and the pressure of the hydrogen gas. This emission is attributed to spontaneous Raman scattering in hydrogen [20]. At a hydrogen pressure

of 5 bar, we obtain an internal spontaneous conversion efficiency of  $1.3 \times 10^{-12}$ , corresponding to an efficiency of about  $7 \times 10^{-15}/(\text{cm bar})$ . The coherent four-wave mixing process can be ten orders of magnitude stronger than this spontaneous process [10].

## IV. CONCLUSION

To conclude, we have demonstrated frequency conversion in high-pressure hydrogen entrapped inside a hollow-core fiber, which increases mode overlap and interaction length by orders of magnitude. Different from all related studies thus far [10], we employ continuous-wave pump fields which do not reduce the bandwidth of the signal photons, but allow for broadband conversion of photons with large coherence time. In future work, we will increase the conversion efficiency through a re-design of the high-pressure vessel and fiber mounts to facilitate higher incoupling efficiency, better power handling, and increased pressure stability.

## V. BACKMATTER

### A. Funding

We acknowledge funding by Deutsche Forschungsgemeinschaft DFG through grant INST 217/978-1 FUGG and through the Cluster of Excellence ML4Q (EXC 2004/1 – 390534769), as well as funding by BMBF through the QuantERA project QuantumGuide.

### B. Acknowledgments

We thank all members of the Cluster of Excellence ML4Q and the QuantumGuide collaboration, as well as Philipp Hänisch, for stimulating discussions.

### C. Disclosures

The authors declare no conflicts of interest.

### D. Data Availability Statement

Data underlying the results presented in this paper are not publicly available at this time but may be obtained from the authors upon reasonable request.

- [1] H. J. Kimble, The quantum internet, *Nature* **453**, 1023 (2008).
- [2] H. Rütz, K.-H. Luo, H. Suche, and C. Silberhorn, Quantum frequency conversion between infrared and ultraviolet, *Phys. Rev. Appl.* **7**, 024021 (2017).
- [3] S. Zaske, A. Lenhard, C. A. Kefler, J. Kettler, C. Hepp, C. Arend, R. Albrecht, W.-M. Schulz, M. Jetter, P. Michler, and C. Becher, Visible-to-telecom quantum frequency conversion of light from a single quantum emitter, *Phys. Rev. Lett.* **109**, 147404 (2012).
- [4] V. Krutyanskiy, M. Meraner, J. Schupp, and B. Lanyon, Polarisation-preserving photon frequency conversion from a trapped-ion-compatible wavelength to the telecom C-band, *Appl. Phys. B* **123**, 228 (2017).
- [5] P. Fisher, R. Cernansky, B. Haylock, and M. Lobino, Single photon frequency conversion for frequency multiplexed quantum networks in the telecom band, *Phys. Rev. Lett.* **127**, 023602 (2021).
- [6] B. A. Bell, K. Wang, A. S. Solntsev, D. N. Neshev, A. A. Sukhorukov, and B. J. Eggleton, Spectral photonic lattices with complex long-range coupling, *Optica* **4**, 1433 (2017).
- [7] P. Y. Zhou, X. M. Dou, X. F. Wu, K. Ding, M. F. Li, H. Q. Ni, Z. C. Niu, D. S. Jiang, and B. Q. Sun, Single-photon property characterization of 1.3  $\mu\text{m}$  emissions from InAs/GaAs quantum dots using silicon avalanche photodiodes, *Scientific Reports* **4**, 3633 (2014).
- [8] R. Ikuta, Y. Kusaka, T. Kitano, H. Kato, T. Yamamoto, M. Koashi, and N. Imoto, Wide-band quantum interface for visible-to-telecommunication wavelength conversion, *Nature Communications* **2**, 537 (2011).
- [9] K. De Greve, L. Yu, P. L. McMahon, J. S. Pelc, C. M. Natarajan, N. Y. Kim, E. Abe, S. Maier, C. Schneider, M. Kamp, S. Höfling, R. H. Hadfield, A. Forchel, M. M. Fejer, and Y. Yamamoto, Quantum-dot spin-photon entanglement via frequency downconversion to telecom wavelength, *Nature* **491**, 421 (2012).
- [10] R. Tyumeneyev, J. Hammer, N. Y. Joly, P. S. J. Russell, and D. Novoa, Tunable and state-preserving frequency conversion of single photons in hydrogen, *Science* **376**, 621 (2022).
- [11] P. J. Winzer, D. T. Neilson, and A. R. Chraplyvy, Fiber-optic transmission and networking: the previous 20 and the next 20 years, *Opt. Express* **26**, 24190 (2018).
- [12] D. Deutsch, C. Buchholz, V. Zolatanosha, K. D. Jöns, and D. Reuter, Telecom C-band photon emission from (In,Ga)As quantum dots generated by filling nanoholes in  $\text{In}_{0.52}\text{Al}_{0.48}\text{As}$  layers, *AIP Advances* **13**, 055009 (2023).
- [13] R. Eramo and M. Matera, Third-harmonic generation in positively dispersive gases with a novel cell, *Appl. Opt.* **33**, 1691 (1994).
- [14] T. Tamaki, K. Midirika, and M. Obara, Phase-matched third-harmonic generation by nonlinear phase shift in a hollow fiber, *Appl. Phys. B* **67**, 59 (1998).
- [15] I. V. Babushkin and J. Herrmann, High energy sub-10 fs pulse generation in vacuum ultraviolet using chirped four wave mixing in hollow waveguides, *Opt. Express* **16**, 17774 (2008).
- [16] M. Cassataro, D. Novoa, M. C. Günendi, N. N. Edavalath, M. H. Frosz, J. C. Travers, and P. S. Russell, Generation of broadband mid-ir and uv light in gas-filled single-ring hollow-core pcf, *Opt. Express* **25**, 7637 (2017).
- [17] H. Rigneault and P. Berto, Tutorial: Coherent Raman light matter interaction processes, *APL Photonics* **3**, 091101 (2018), [https://pubs.aip.org/aip/app/article-pdf/doi/10.1063/1.5030335/19920671/091101\\_1\\_1.5030335.pdf](https://pubs.aip.org/aip/app/article-pdf/doi/10.1063/1.5030335/19920671/091101_1_1.5030335.pdf).
- [18] D. W. Shipp, F. Sinjab, and I. Notinger, Raman spectroscopy: techniques and applications in the life sciences, *Advances in Optics and Photonics* **9**, 315 (2017).
- [19] Z.-Y. Tian, V. B. Mbayachi, X. Zhang, M. Khalil, and D. A. Ayejoto, Coherent anti-stokes raman scattering, in *Advanced Diagnostics in Combustion Science* (Springer Nature Singapore, Singapore, 2023) pp. 179–222.
- [20] R. W. Boyd, Chapter 1 - the nonlinear optical susceptibility, in *Nonlinear Optics (Third Edition)*, edited by R. W. Boyd (Academic Press, Burlington, 2008) third edition ed.
- [21] A. Aghababaei, C. Biesek, F. Vewinger, and S. Stellmer, Frequency conversion in pressurized hydrogen, *Opt. Lett.* **48**, 45 (2023).
- [22] R. Grössle, B. Bornschein, A. Kraus, S. Mirz, and S. Wozniowski, Minimal and complete set of descriptors for IR-absorption spectra of liquid H<sub>2</sub>-D<sub>2</sub> mixtures, *AIP Advances* **10**, 055108 (2020), [https://pubs.aip.org/aip/adv/article-pdf/doi/10.1063/1.5111000/12840001/055108\\_1\\_online.pdf](https://pubs.aip.org/aip/adv/article-pdf/doi/10.1063/1.5111000/12840001/055108_1_online.pdf).
- [23] A. Hamer, S. M. R. Tabar, P. Yashwantrao, A. Aghababaei, F. Vewinger, and S. Stellmer, Frequency conversion to the telecom o-band using pressurized hydrogen, *Opt. Lett.* **49**, 506 (2024).
- [24] Y.-S. Wang, K.-B. Li, C.-F. Chang, T.-W. Lin, J.-Q. Li, S.-S. Hsiao, J.-M. Chen, Y.-H. Lai, Y.-C. Chen, Y.-F. Chen, C.-S. Chuu, and I. A. Yu, Temporally ultralong biphotons with a linewidth of 50 kHz, *APL Photonics* **7**, 126102 (2022).
- [25] W. Belardi, *Hollow core optical fibers* (MDPI - Multidisciplinary Digital Publishing Institute, 2019) <https://doi.org/10.3390/books978-3-03921-089-3>.
- [26] R. F. Ando, A. Hartung, B. Jang, and M. A. Schmidt, Approximate model for analyzing band structures of single-ring hollow-core anti-resonant fibers, *Opt. Express* **27**, 10009 (2019).
- [27] L. R. Murphy and D. Bird, Azimuthal confinement: the missing ingredient in understanding confinement loss in anti-resonant, hollow-core fibers, *Optica* **10**, 854 (2023).
- [28] F. Yu and J. C. Knight, Negative curvature hollow-core optical fiber, *IEEE Journal of Selected Topics in Quantum Electronics* **22**, 146 (2016).
- [29] A. Taranta, E. Numkam Fokoua, S. Abokhamis Mousavi, J. R. Hayes, T. D. Bradley, G. T. Jasion, and F. Poletti, Exceptional polarization purity in anti-resonant hollow-core optical fibres, *Nature Photonics* **14**, 504 (2020).
- [30] P. S. J. Russell, P. Hölzer, W. Chang, A. Abdolvand, and J. C. Travers, Hollow-core photonic crystal fibres for gas-based nonlinear optics, *Nature Photonics* **8**, 278 (2014).
- [31] A. Bahari, K. Sower, K. Wang, Z. Han, J. Florence, Y. Wang, S. Gao, H. W. H. Lee, M. Scully, A. Zheltikov, and A. Sokolov, Background-penalty-free waveguide enhancement of cars signal in air-filled anti-resonance hollow-

- core fiber, *Opt. Lett.* **47**, 4339 (2022).
- [32] M. Afsharnia, S. Junaid, S. Saravi, M. Chemnitz, K. Wondraczek, T. Pertsch, M. A. Schmidt, and F. Setzpfandt, Generation of infrared photon pairs by spontaneous four-wave mixing in a  $\text{CS}_2$ -filled microstructured optical fiber, *Scientific Reports* **14**, 977 (2024).
- [33] M. K. Mridha, D. Novoa, P. Hosseini, and P. S. Russell, Thresholdless deep and vacuum ultraviolet raman frequency conversion in hydrogen-filled photonic crystal fiber, *Optica* **6**, 731 (2019).
- [34] Y. Cui, X. Tian, B. Rao, H. Li, W. Huang, W. Pei, M. Wang, Z. Chen, and Z. Wang, A 110 w fiber gas raman laser at 1153 nm, *High Power Laser Science and Engineering* **11**, e10 (2023).
- [35] F. Couny, F. Benabid, and P. S. Light, Subwatt threshold cw raman fiber-gas laser based on  $\text{H}_2$ -filled hollow-core photonic crystal fiber, *Phys. Rev. Lett.* **99**, 143903 (2007).
- [36] P. Arcos, A. Mena, M. Sánchez-Hernández, E. Arrospide, G. Aldabaldetrekú, M. A. Illarramendi, J. Zubia, and D. Novoa, Stimulated raman scattering and molecular modulation in anti-resonant hollow-core fibres (2024), <https://arxiv.org/abs/2407.06996>, arXiv:2407.06996 [physics.optics].
- [37] W. B. Gao, P. Fallahi, E. Togan, J. Miguel-Sanchez, and A. Imamoglu, Observation of entanglement between a quantum dot spin and a single photon, *Nature* **491**, 426 (2012).
- [38] J. Liu, R. Su, Y. Wei, B. Yao, S. Filipe Covre da Silva, Y. Yu, J. Iles-Smith, K. Srinivasan, A. Rastelli, J. Li, and X. Wang, A solid-state source of strongly entangled photon pairs with high brightness and indistinguishability, *Nat. Nanotechnol.* **14**, 586 (2019).
- [39] H. Wang, H. Hu, T.-H. Chung, J. Qin, X. Yang, J.-P. Li, R.-Z. Liu, H.-S. Zhong, Y.-M. He, X. Ding, Y.-H. Deng, Q. Dai, Y.-H. Huo, S. Höfling, C.-Y. Lu, and J.-W. Pan, On-demand semiconductor source of entangled photons which simultaneously has high fidelity, efficiency, and indistinguishability, *Phys. Rev. Lett.* **122**, 113602 (2019).
- [40] B. Joecker, P. Cerfontaine, F. Haupt, L. R. Schreiber, B. E. Kardynał, and H. Bluhm, Transfer of a quantum state from a photonic qubit to a gate-defined quantum dot, *Phys. Rev. B* **99**, 205415 (2019).
- [41] M. Zeisberger, A. Hartung, and M. A. Schmidt, Understanding dispersion of revolver-type anti-resonant hollow core fibers, *Fibers* **6**, 10.3390/fib6040068 (2018).
- [42] V. Zuba, H. C. H. Mulvad, R. Slavík, H. Sakr, F. Poletti, D. J. Richardson, and E. N. Fokoua, Limits of coupling efficiency into hollow-core antiresonant fibres, *Journal of Lightwave Technology* **41**, 6374 (2023).
- [43] W. K. Bischel and M. J. Dyer, Temperature dependence of the raman linewidth and line shift for the Q(1) and Q(0) transitions in normal and para- $\text{H}_2$ , *Phys. Rev. A* **33**, 3113 (1986).
- [44] E. C. Looi, J. C. Stryland, and H. L. Welsh, Pressure shifts in the vibrational raman spectra of hydrogen and deuterium, 315-85 k, *Canadian Journal of Physics* **56**, 1102 (1978).
- [45] A. D. May, V. Degen, J. C. Stryland, and H. L. Welsh, The Raman effect in gaseous hydrogen at high pressures, *Canadian Journal of Physics* **39**, 1769 (1961).
- [46] M. Ziemieniczuk, A. M. Walser, A. Abdolvand, and P. S. J. Russell, Intermodal stimulated raman scattering in hydrogen-filled hollow-core photonic crystal fiber, *J. Opt. Soc. Am. B* **29**, 1563 (2012).